Catalysis Today 146 (2009) 299–307

Contents lists available at ScienceDirect

Catalysis Today

journal homepage: www.elsevier.com/locate/cattod

Temperature dependence of electrochemically promoted NO reduction by C_3H_6 under stoichiometric conditions using Me/YSZ/Au (Me = Rh, RhPt, Pt) electrochemical catalysts

Y. Sakamoto [a,*], K. Okumura [a], H. Shinjoh [a], M. Lepage [b], S. Brosda [c]

[a] Toyota Central R&D Laboratory Inc. Catalysis Division, Nagakute, Aichi 480-1192, Japan
[b] Toyota Motor Europe NV/SA, Technical Centre, Hoge Wei 33, B1930 Zaventem, Belgium
[c] Department of Chemical Engineering, Caratheodory 1 Street, University of Patras, GR-26504 Patras, Greece

ARTICLE INFO

Article history:
Available online 29 April 2009

Keywords:
Electrochemical catalyst
Non-Faradaic electrochemical modification of catalytic activity
Electrochemical promotion effect
NO_x selective reduction reaction
HC oxidation
NO reduction

ABSTRACT

Temperature dependence of electrochemical promotion in C_3H_6–NO–O_2 reaction under stoichiometric conditions was investigated using Me/yttria-stabilized zirconia (YSZ)/Au (Me = Rh, RhPt, Pt) electrochemical catalysts, wherein electrodes were deposited by a sputtering method. Influences of the applied potential, the sintering extent of YSZ substrate, and the precious metal used for the electrode were investigated.

Based on the analysis of catalytic reaction and electrode surface state, the longer sintering of YSZ substrate induced a positive effect for non-Faradaic electrochemical promotion of C_3H_6 oxidation by favoring oxygen spillover, and a negative effect for Faradaic electro-reduction of NO due to decrease in electrical conductivity. We postulated that RhPt electrode showed catalytic activity using the synergistic effect of Pt and Rh; however, higher activity than pure Rh electrode was not observed.

1. Introduction

The use of electrochemical catalysts for automotive exhaust gas purification was investigated intently [1–3]. It has been proposed that electrochemical catalysts may solve problems encountered by automotive catalysts, because their catalytic activity and selectivity are controlled with the applied potential.

Electrochemical catalysts can function in two ways: (1) as electrodes in an electrochemically activated reaction [4,5], and (2) as electrodes enhancing the catalytic activity and modifying the reaction selectivity [6,7]. In the latter case, the non-Faradaic electrochemical modification of catalytic activity (NEMCA) or electrochemical promotion (EP) effect is elucidated, because the consumption of electricity is extremely low compared with the increase in turnover frequency due to applied current. NEMCA effect has been observed for the oxidation of hydrocarbons and carbon monoxide [8] and NO_x selective reduction reactions [9]. Because both reactions are related to automotive exhaust gas purification, the relevance of NEMCA effect for such applications necessitates a study. To know the differences between Rh electrode on NEMCA and Rh dispersed particle, we have already compared turnover frequencies (TOFs), which relate the reaction rate to the number of catalytically active sites between a Rh electrochemical catalyst and a dispersed Rh/yttria-stabilized zirconia (YSZ) catalyst [9]. It was observed that the values of TOFs of the dispersed Rh/YSZ catalyst are intermediate between the corresponding TOFs on the unpromoted and electropromoted Rh catalyst-electrode films. This result indicates that electropromoted catalysts decrease the amount of precious metals required in automotive catalysts. However, at this stage, NEMCA effect has not been characterized to an extent that it could be applied in the purification of automotive exhaust gases.

NEMCA effect has been generally evaluated by measuring the influence of changes in the applied potential on the reaction rate under static temperature conditions. On the other hand, automotive catalysts are usually evaluated by measuring the changes in the reactants' conversion as a function of temperature using static or transient gas compositions. It is possible to evaluate the potential of NEMCA by studying the effect of temperature at constant gas compositions. The dependence of NEMCA on the reaction temperature of Pt/Na–Al_2O_3/Au system has been investigated in this manner [10].

Furthermore, the catalytic performance of automotive catalysts is strongly affected by the size of precious metal particles, the surface area, and the surface condition of the support influencing the active sites [11–13]. In NEMCA studies, it is difficult to investigate the role of oxygen ion conductor. Therefore, we studied intently the effect of sintering duration on the YSZ solid electrolyte.

* Corresponding author. Tel.: +81 561 63 5312; fax: +81 561 63 6150.
E-mail address: sakamoto@mosk.tytlabs.co.jp (Y. Sakamoto).

0920-5861/$ – see front matter © 2009 Elsevier B.V. All rights reserved.
doi:10.1016/j.cattod.2009.03.024

Table 1
Electrochemical catalysts. YSZ sintering was performed in air and the electrodes were deposited by sputtering.

Sample	Work electrode	Counter electrode	YSZ sintering condition
Rh/10YSZ/Au	200 nm Rh	300 nm Au	1500 °C × 5 h
Rh/YSZ/Au			1500 °C × 1 h
Pt/YSZ/Au	200 nm Pt		
RhPt/YSZ/Au	200 nm Rh/200 nm Pt		

The effect of the electrode material affecting the NEMCA phenomenon was also studied. Three types of electrodes were selected for this purpose: Rh, Pt, and PtRh. Because it was known that the catalytic rate of propane oxidation of Pt electrodes is 300 times higher than that of Rh electrodes [14], and that the reduction of NO_x by ethylene in the presence of O_2 is electropromoted predominantly by positive currents on Rh [15,16], few synergistic effects between Rh and Pt similar to that observed in PtRh alloy catalysts [17–19] were anticipated.

2. Experimental

The electrochemical catalysts consist of a YSZ circular plate with two electrodes. YSZ plate was obtained by pressing the YSZ powder (TZ-8Y; Tosoh Corporation, Tokyo, Japan) into a disc of 20 mm diameter and 1 mm thickness using a cold isostatic press at 3000 kg/cm^2. Then, it was sintered in air at 1480 °C for 1 h and 10 h, and contracted to 80% of the original size in terms of its thickness and diameter.

The electrodes were deposited on both sides by magnetron sputtering in an Ar gas atmosphere. For example, the RhPt electrode was obtained by depositing a 200 nm Rh film on a 200 nm thick Pt layer. The electrical contact was established using Au wires (0.2 mm in diameter) fixed on both electrodes with an Au paste (TR-1592; Tanaka Kikinzoku Kogyo K.K., Tokyo, Japan). The sample details are summarized in Table 1. In this study, no reference electrode was used.

Fig. 1 shows XRD patterns and scanning electron microscope (SEM) photographs of bare YSZ plates before and after sintering in air. It can be inferred from the figure that the grain size increased and the surface roughness decreased by increasing the aging duration. And the XRD patterns indicated the crystallite size of YSZ after sintering was almost same. This tendency was also observed by Dong et al. for a YSZ film used in a solid oxide fuel cell [20].

The catalytic activity was measured using the setup illustrated in Fig. 2. The reactor was a quartz tube having an inner diameter of 20 mm and a length of 400 mm. It was partially filled with small quartz tubes of 5 mm outer diameter, 3.5 mm inner diameter, and 5 mm length to pre-heat the reactant gases. The heating was conducted using an IR radiation furnace where the reactor was positioned. The sample was placed in the middle of the tube, and the gas was fed from the bottom of the reactor. The composition of the gas mixture was as follows: 1000 ppm NO + 1000 ppm C_3H_6 + 0.4% O_2, with the rest being He, which corresponded to a stoichiometric condition for the following reaction.

$$NO + 4O_2 + C_3H_6 \rightarrow 0.5N_2 + 3H_2O + 3CO_2 \quad (1)$$

The total flow rate was 60 cc/min. To avoid effects such as the adsorption of gases at a low temperature, contamination of the electrode, and changes due to thermal aging while measuring, the catalyst sample was pre-treated in the reactant gas flow by increasing the temperature at a rate of 10 °C/min up to 600 °C, and thereafter, maintaining it at 600 °C for 10 min. During pre-treatment, the electrode potential was already set at the required voltage for the following experiment. After pre-treatment, the conversion percentage was continuously determined while cooling was conducted in the temperature range of 600–200 °C at a rate of 10 °C/min. The effluent gas composition was analyzed using a quadrupole mass spectrometer (Massmate; ULVAC, Inc., Kanagawa, Japan). C_3H_6, NO, and O_2 were monitored at mass numbers m/e = 41, 30, and 32, respectively. The applied potential was controlled, and the current was measured using a digital constant voltage power supply (type 2400; Keithley Instruments Inc., Ohio, USA).

After measuring the gas flow, the inlet gas flow was directly connected to the quadrupole mass spectrometer without it going through the reactor and measured as the intensity of the bypass for C_3H_6 and NO. The C_3H_6 and NO conversions were calculated from the mass intensity, with and without going through the reactor, using equation (2):

$$X = \frac{(I_0 - I)}{(I_0 - I_{bp})} \times 100 \quad (2)$$

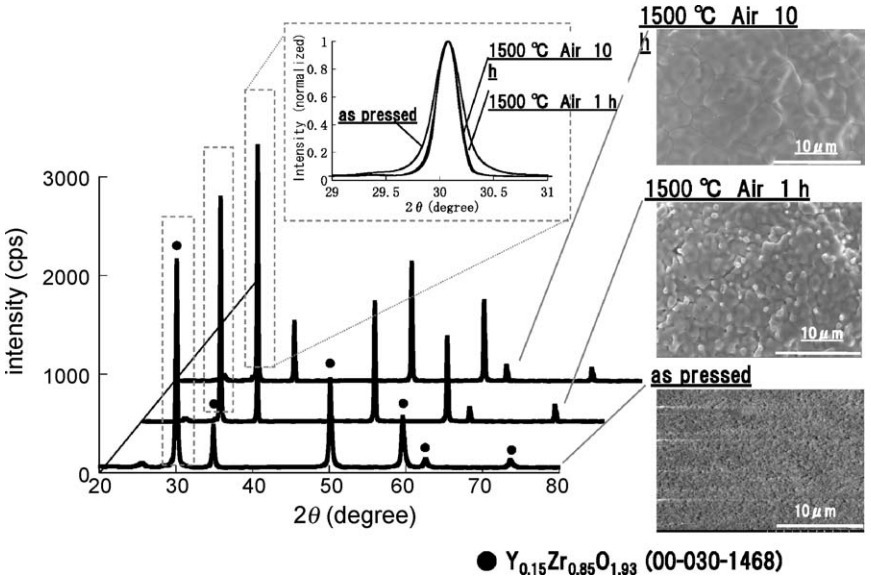

Fig. 1. XRD and SEM of pressed and sintered YSZ before sputtering electrode. The longer duration increased the grain size of YSZ.

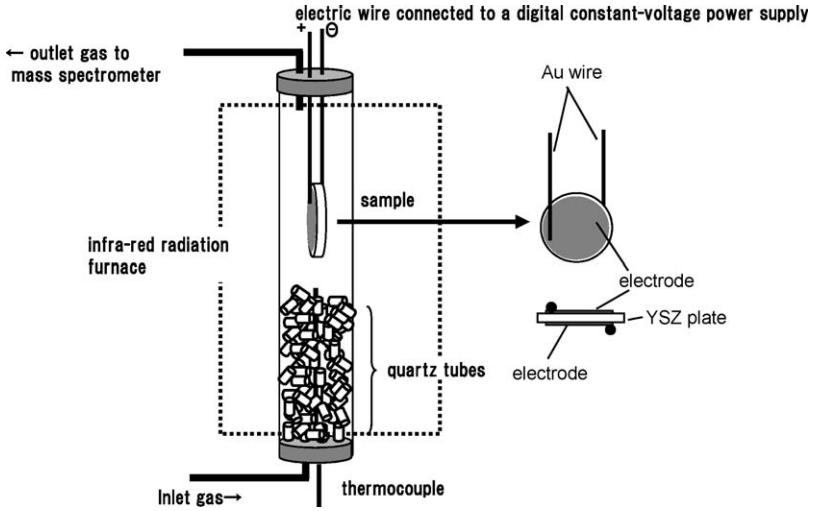

Fig. 2. Schematic of the setup for catalytic activity measurements.

where X (%) is conversion, I is mass intensity, I_0 is the mass intensity of the background, and I_{bp} is the intensity of the bypass for C_3H_6 and NO.

After measuring the catalytic activity, we investigated each electrode using a SEM and X-ray photoelectron spectroscopy (XPS) to understand the relation between catalytic activity and electrode state.

3. Results

The results of C_3H_6 and NO conversion for NEMCA effect measurement on Rh/YSZ/Au sample are shown in Fig. 3. At the high temperature above 400 °C under open circuit conditions, the C_3H_6 conversion percentage increased to 60% (a thin solid line in Fig. 3(a)) in a way similar to that observed using traditional precious metal dispersed catalysts. The temperature dependence of NO conversion exhibited a maximum (30–40%) in the temperature range of 250–400 °C (a thin solid line in Fig. 3(b)). This tendency in NO conversion has been observed for stoichiometric conditions in case of Pt/YSZ [21]. A 100% C_3H_6 conversion was not achieved even at 550 °C on our experiments. Presumably, a part of the feed gases could not touch enough to react due to the large space between the catalyst and the tube reactor.

When we applied a potential of +2 V to the Rh working electrode, the oxidation of C_3H_6 was enhanced in the entire temperature range under investigation (a thick solid line in Fig. 3(a)), whereas an improvement in NO conversion was limited to a temperature ranging from 250 to 400 °C (a thick solid line in Fig. 3(b)). When a potential of −2 V was applied to the Rh electrode, both C_3H_6 and NO conversion reduced in the temperature ranging from 200 to 375 °C and 200 to 325 °C, respectively (a dotted solid line in Fig. 3(a) and (b)). These responses to the applied potential are similar to that observed by Pliangos et al. [16].

On increasing the temperature above 350 °C with an applied potential of −2 V, the percentage of NO conversion increased from 40 to 70% (Fig. 3(b)), and a relatively intense current flowed compared to that for +2 V (Fig. 4(a)). This phenomenon can be explained by reducing the electrical resistance of the Rh electrode, because the oxidized Rh electrode is electrochemically reduced to metallic Rh by applying a −2 V potential. This intense current is accompanied by an increased NO conversion due to the electrochemical NO decomposition reaction [4].

We analyzed typical NEMCA parameters for the Rh/YSZ/Au sample described in Fig. 4 using the rate enhancement factor ρ and the apparent Faradaic efficiency Λ, which are defined as follows:

$$\rho = \frac{r}{r_o} \tag{3}$$

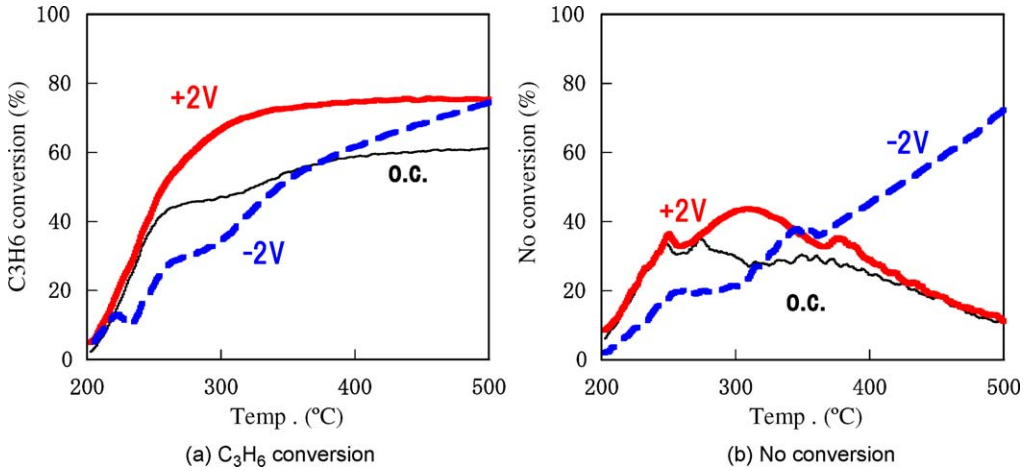

Fig. 3. Effect of applied potential on C_3H_6 and NO conversion for Rh/YSZ/Au. The thin lines indicate conversions for open circuit, the thick lines indicate conversions on applying +2 V, and the thick and dashed lines indicate conversions on applying −2 V.

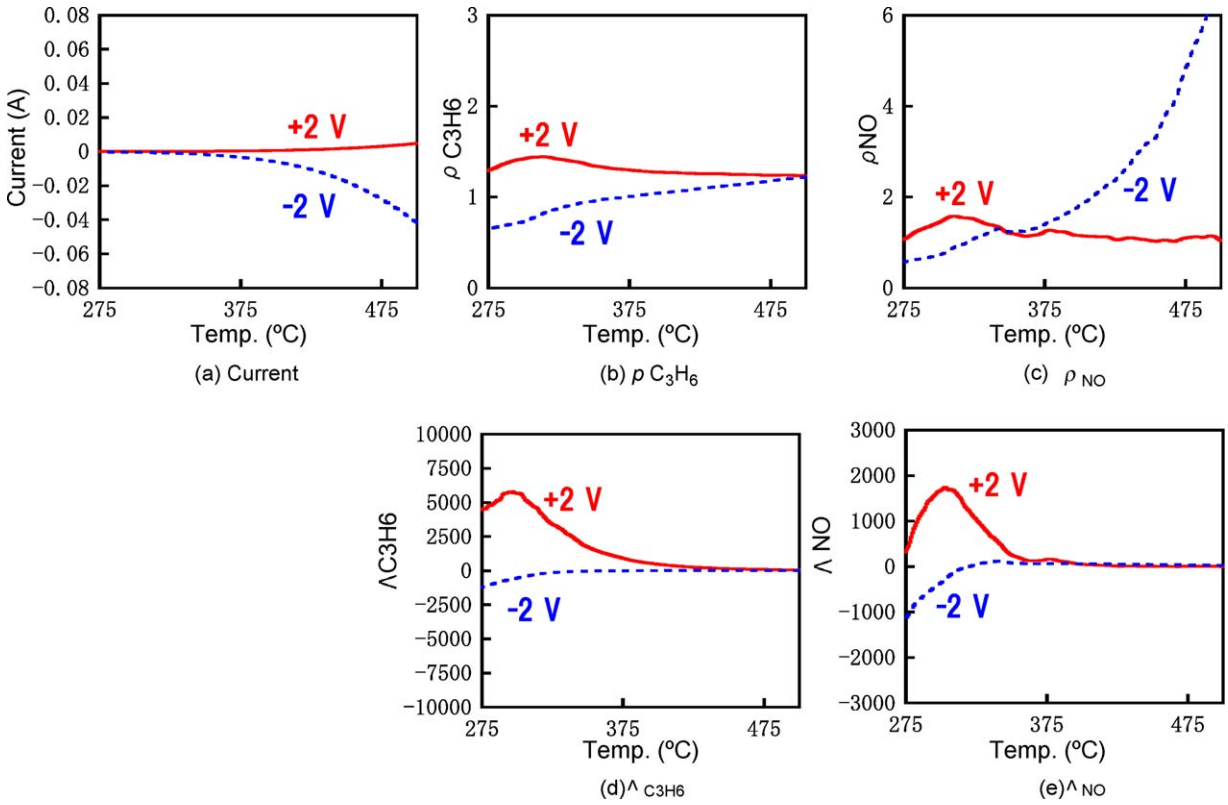

Fig. 4. Temperature dependence of current, rate enhancement factor ρ and apparent Faradaic efficiency Λ for Rh/YSZ/Au.

$$\Lambda = \frac{\Delta r}{(I/2F)} \tag{4}$$

where r is the electropromoted catalytic rate (mol O/s) and r_o is the unpromoted (open-circuit) catalytic rate (mol O/s), Δr is the potential-induced change in catalytic rate(mol O/s), I is the applied current (A), and F is Faraday's constant (96480 C/mol). We assumed the following reactions for C_3H_6 oxidation and NO reduction and then calculated ρ and Λ. It was not possible to calculate the value of ρ and Λ below 275 °C due to a small value of the current and the conversion of NO and C_3H_6.

$$C_3H_6 + 4.5O_2 \rightarrow 3CO_2 + 3H_2O \tag{5}$$

$$NO \rightarrow 0.5N_2 + 0.5O_2 \tag{6}$$

The ρ value for NO reduction upon application of −2 V (Fig. 4(c)) was very large due to Faradaic NO reduction, which is further confirmed by the fact that Λ for NO on applying −2 V was very small, as illustrated by the dotted line in Fig. 5(e). As illustrated in Fig. 5, Λ values displayed a maximum value for C_3H_6 oxidation and NO reduction at about 300 °C on applying +2 V (Fig. 4(d) and (e)).

The influence of the sintering duration of YSZ electrolyte was also investigated. The temperature dependence of the catalytic activity under open circuit conditions was studied using the same gas mixture of 1000 ppm NO + 1000 ppm C_3H_6 + 0.4% O_2 on Rh/10YSZ/Au. According to Fig. 5, the catalytic activity for Rh/10YSZ/Au was higher than that for Rh/YSZ/Au irrespective of the applied potential except for the condition where the temperature was above 400 °C at an applied potential of −2 V potential. A longer

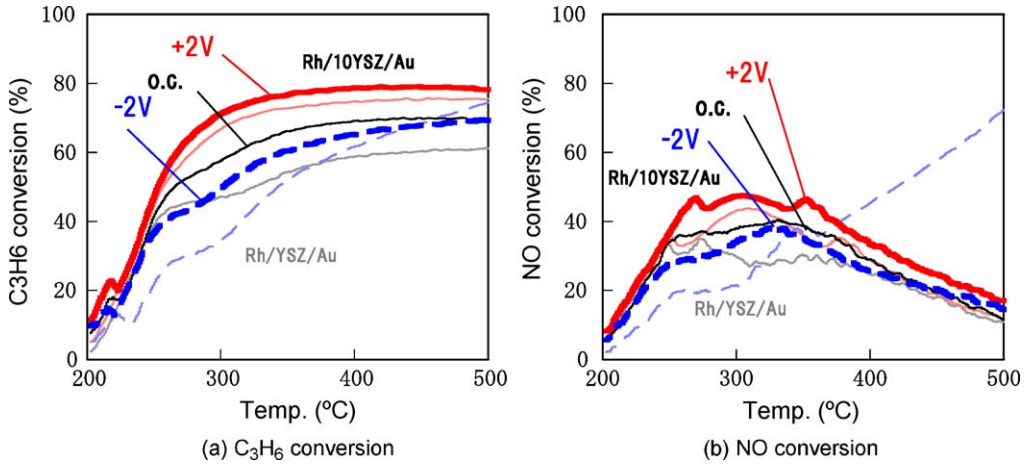

Fig. 5. Effect of applied potential on C_3H_6 and NO conversion for Rh/10YSZ/Au. The thin lines indicate conversions for open circuit, the thick lines indicate conversions on applying +2 V, and the thick and dashed lines indicate conversions on applying −2 V. The faint color lines indicate the conversion for Rh/YSZ/Au.

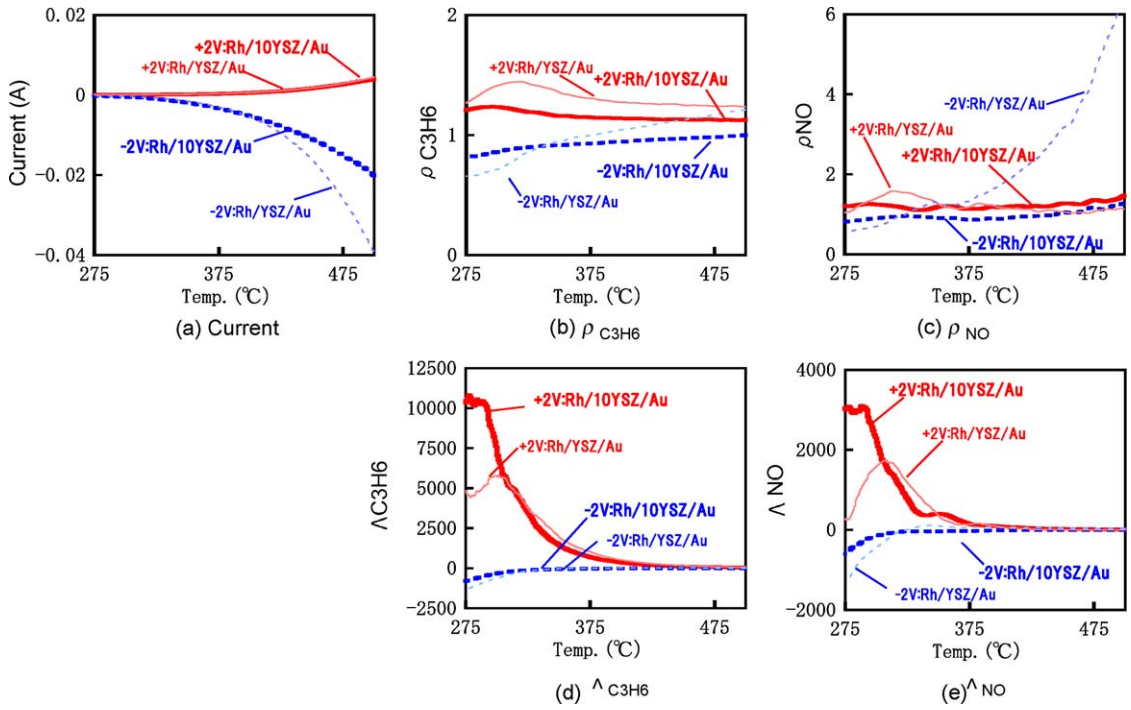

Fig. 6. Temperature dependence of current, rate enhancement factor ρ, and apparent Faradaic efficiency Λ for Rh/10YSZ/Au. The faint color lines indicate the ρ and Λ for Rh/YSZ/Au.

sintering duration of YSZ inhibited the NO Faradaic reduction above 400 °C with a −2 V potential; whereas a decrease of C_3H_6 and NO conversion with an applied potential of −2 V below 250 °C did not occur.

The currents curve with the applied potential of +2 V on Rh/YSZ/Au and Rh/10YSZ/Au (the solid lines in Fig. 6(a)) looked like almost same while the amount of current with the applied potential of −2 V on Rh/10YSZ/Au (the thin dotted line in Fig. 6(a)) was larger than that of Rh/10YSZ/Au (the thick dotted line in Fig. 6(a)). The large amount of current with the applied potential of −2 V on Rh/10YSZ/Au can reduce NO electrically at the high temperature. The ρ of Rh/10YSZ/Au for C_3H_6 oxidation (the thick solid line in Fig. 6(b)) was smaller than that of Rh/YSZ/Au (the thin solid line in Fig. 6(b)). The smaller ρ value of C_3H_6 oxidation for Rh/10YSZ/Au was caused by the low Δr value due to the high C_3H_6 conversion of Rh/10YSZ/Au without applied potential ("o.c." shown in Fig. 5(a)). From the fact of the high C_3H_6 conversion of Rh/10YSZ/Au without applied potential, the Rh/10YSZ/Au may be already electropromoted under the open circuit condition. The Λ of C_3H_6 oxidation for Rh/10YSZ/Au with +2 V potential below 300 °C was higher than that for Rh/YSZ/Au potential (Fig. 6(d)). Some readers may fell the large differences of Λ strange because the current looks similar and ρ for Rh/YSZ/Au is higher than that for Rh/10YSZ/Au. We suppose that the small difference of current caused the large differences of Λ. For example, the current values at 280 °C on applying +2 V for Rh/YSZ/Au and Rh/10YSZ/Au were 60.2 μA and 26.8 μA respectively. As a result, the lower current of Rh/10YSZ/Au indicated the higher ρ of Rh/10YSZ/Au according to equation (4).

When the potential of +2 V was applied to Rh/10YSZ/Au, the peak of the ρ for NO reduction around 300 °C, which was seen on the case of Rh/YSZ/Au, was not seen (the thick solid line in Fig. 6(c)). The large Λ of NO reduction for Rh/10YSZ/Au with +2 V potential below 300 °C was the same as the case of C_3H_6 oxidation (Fig. 6(e)).

Fig. 7 describes the results obtained on RhPt/YSZ/Au, which are very similar to those obtained on Rh/YSZ/Au (Fig. 3). For example,

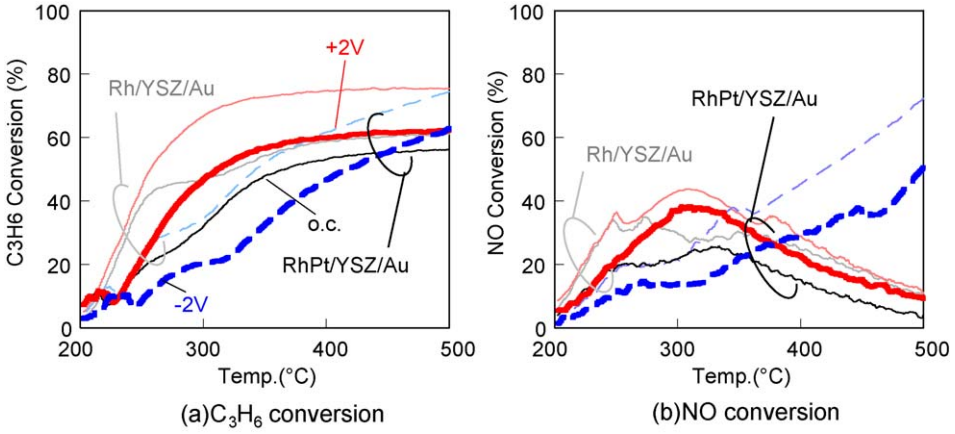

Fig. 7. Effect of applied potential on C_3H_6 and NO conversion for RhPt/YSZ/Au. The thin lines indicate conversions for open circuit, the thick lines indicate conversions on applying +2 V, and the thick and dashed lines indicate conversions on applying −2 V. The faint color lines show the conversion for Rh/YSZ/Au.

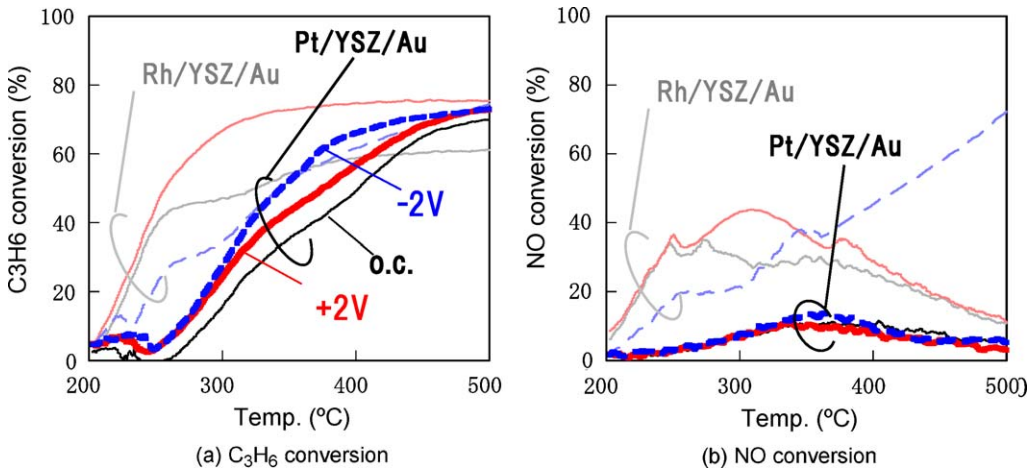

Fig. 8. Effect of applied potential on C_3H_6 and NO conversion for Pt/YSZ/Au. The thin lines indicate conversions for open circuit, the thick lines indicate conversions on applying +2 V, and the thick and dashed lines indicate conversions on applying −2 V. The faint color lines show the conversion for Rh/YSZ/Au.

applying a +2 V potential increased the conversion of C_3H_6 and NO, and applying a −2 V potential decreased the conversion of C_3H_6 up to at least 450 °C and of NO up to 350 °C followed by an increase above 400 °C. Though RhPt/YSZ/Au showed similar behaviors with Rh/YSZ/Au like above, there were some differences between RhPt/YSZ/Au and Rh/YSZ/Au: the ρ of C_3H_6 with +2 V potential below 300 °C increased, while ρ of C_3H_6 with −2 V potential above 300 °C decreased. The increase of ρ of NO with −2 V potential began at a lower temperature, and ρ for RhPt/YSZ/Au below 300 °C for both C_3H_6 and NO was larger than ρ for Rh/YSZ/Au. These differences will be discussed further in the next section.

Fig. 8 illustrates the plot of C_3H_6 and NO conversion with respect to temperature for Pt/YSZ/Au. The catalytic activity of Pt/YSZ/Au sample was low compared with that for the Rh/YSZ/Au sample, irrespective of the applied potential. In case of Pt/YSZ/Au, the difference in catalytic activity with and without the applied potential was small, and at applied potentials of +2 V and −2 V, the catalytic activity was enhanced. These results significantly differed from those obtained for Rh/YSZ/Au that showed that the catalytic reaction increased on applying +2 V and decreased on applying −2 V.

In order to know the reason for the difference in the catalytic activity and electrocatalyst behavior for each catalyst, we investigated the surface morphology and state using SEM and XPS. Fig. 9 illustrates the SEM image of Rh/YSZ/Au, Rh/10YSZ/Au, RhPt/YSZ/Au, and Pt/YSZ/Au. The surface morphology of Rh/YSZ/Au and RhPt/YSZ/Au were very similar; however, they significantly differed for Rh/10YSZ/Au and Pt/YSZ/Au. Rh and RhPt electrode of Rh/YSZ/Au and RhPt/YSZ/Au adhered tightly on the YSZ substrate (Fig. 9(a) and (c)). On the other hand, the Rh electrode of Rh/10YSZ/

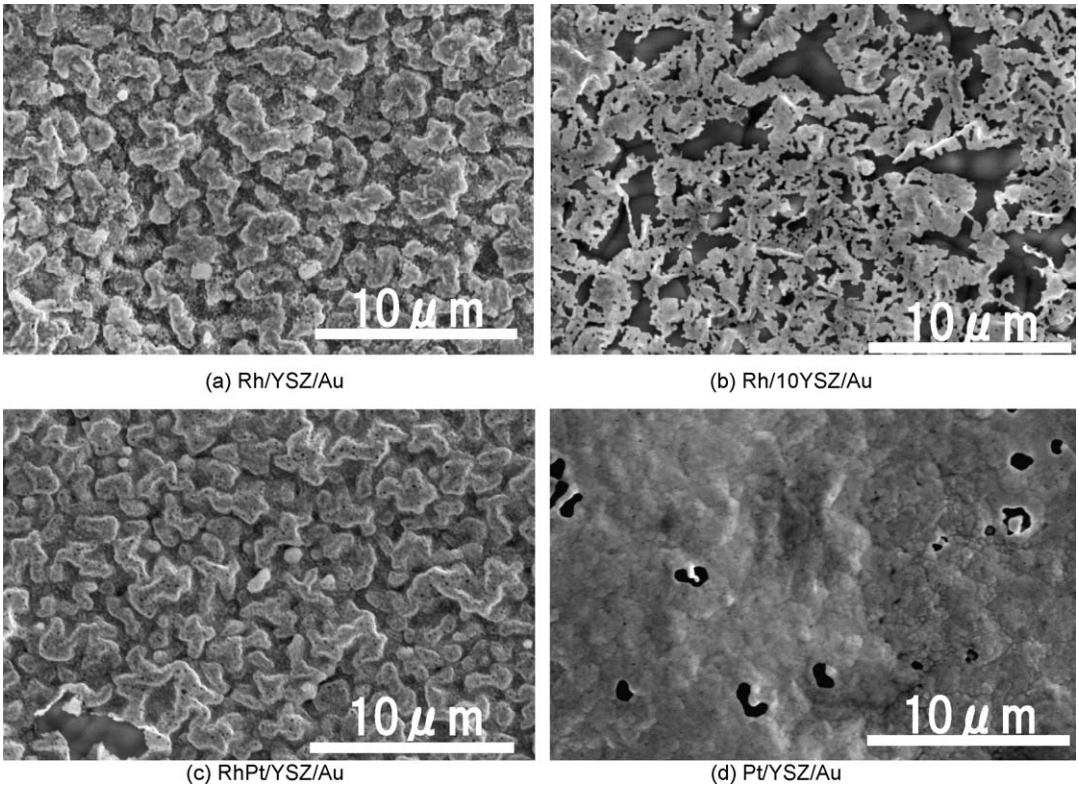

Fig. 9. SEM analysis of electrodes. (a) Rh/YSZ/Au, (b) Rh/10YSZ/Au, (c) RhPt/YSZ/Au and (d) Pt/YSZ/Au.

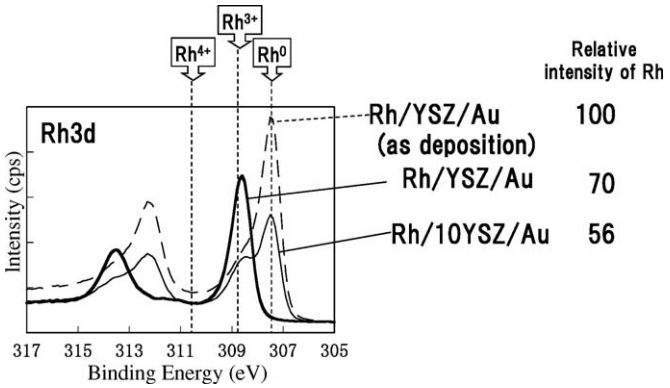

Fig. 10. XPS analysis for Rh electrode. The thick line indicates the Rh/YSZ/Au, the thin line indicates the Rh/10YSZ/Au, and the thin dashed line indicates the Rh/YSZ/Au as deposition. The relative intensity of Rh was normalized by the Rh intensity for Rh/YSZ/Au.

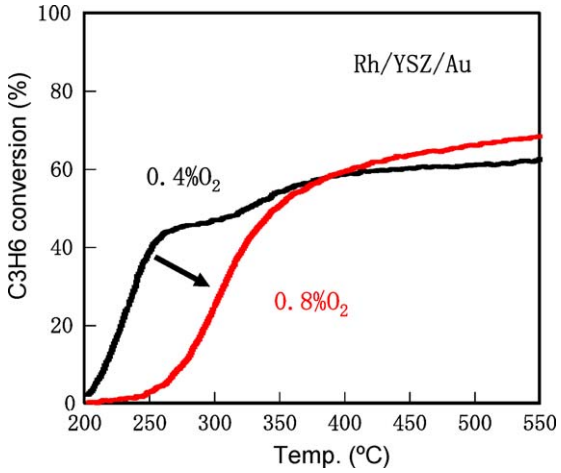

Fig. 12. Effect of oxygen concentration on C_3H_6 conversion of Rh/YSZ/Au and Pt/YSZ/Au under the open circuit condition.

Au had nearly peeled from the YSZ substrate (Fig. 9(b)). The Pt electrode of Pt/YSZ/Au was smooth, and there were several holes of a few micrometers in size (Fig. 9(d)).

XPS results were compared for the surface state of Rh electrode (Fig. 10). XPS analysis revealed that Rh electrode as deposition was in the metal state, but Rh electrode of Rh/YSZ/Au was fully oxidized. On the other hand, Rh electrode of Rh/10YSZ/Au was not fully oxidized and remained in the metal state of Rh. Furthermore, it was observed for both SEM and XPS analyses that the Rh electrode of Rh/10YSZ/Au was sintered, as indicated by the intensity of Rh and rhodium oxides. Fig. 11 shows the result of XPS analysis for the electrodes of Rh/YSZ/Au, Pt/YSZ/Au, and RhPt/YSZ/Au. Only Rh peak was observed in the analysis of RhPt/YSZ/Au, and the Rh was fully oxidized to the same extent as the electrode of Rh/YSZ/Au. The electrode of RhPt/YSZ/Au was completely covered with Rh.

4. Discussion

Based on the results obtained, the differences between the catalytic and electric behavior were discussed from the perspective of YSZ-sintering duration and electrode-type.

According to the previous study [22], C_3H_6 is classified as an electron donor [23], and both O_2 [7,24] and NO are classified as electron acceptors. A negative potential leads to a decrease in the electrode work function and may weaken the chemical bonds of the electrode with respect to electron-donor adsorbates, such as C_3H_6, while strengthening electrodes with an electron-acceptor of O_2 and NO [25,26]. Moreover, it was observed that an Rh electrode lost catalytic activity at a temperature ranging from 300 to 400 °C in the presence of a gas mixture containing 1000 ppm C_3H_6 + 1000 ppm NO + 0.5% O_2 (due to oxidation of Rh surface) and that a positive current enhanced the catalytic activity [27]. This "oxygen poison" for a Rh electrode was also confirmed by our investigation of the effect of oxygen concentration on the catalytic activity, as illustrated in Fig. 12. When oxygen concentration was increased from 0.4% to 0.8%, the C_3H_6 conversion was decreased at the temperature range from 200 to 360 °C. The positive potential for a Rh electrode weakens the chemical bonds with oxygen and promotes catalytic activity. Conversely, it is expected that a negative potential strengthens the chemical bonds with oxygen and leads to a loss in catalytic activity.

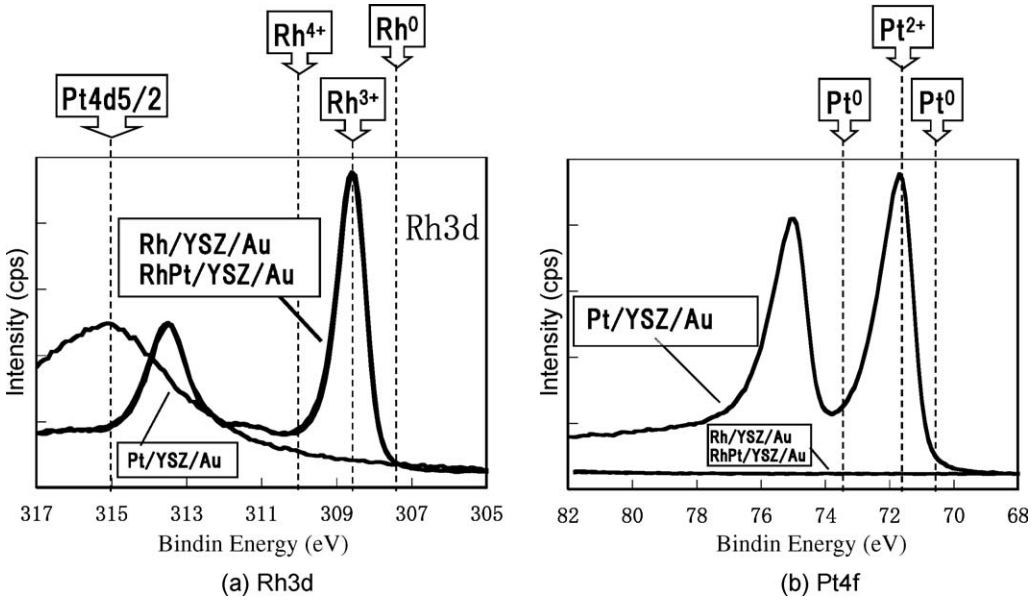

Fig. 11. XPS analysis for the electrode of Rh/YSZ/Au, RhPt/YSZ/Au and Pt/YSZ/Au. The spectrum of Rh3d and Pt4f for Rh/YSZ/Au and RhPt/YSZ/Au were the same and are superimposed.

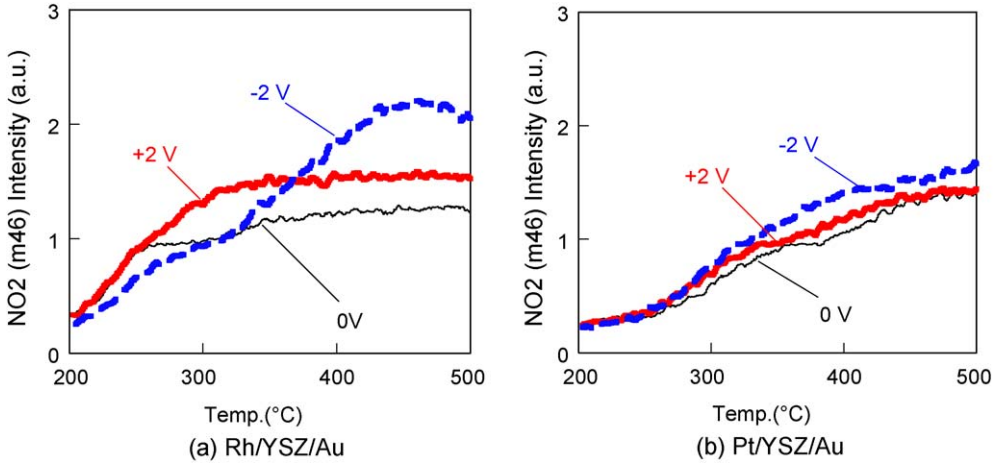

Fig. 13. NO_2 (m/e = 46) yielding for Rh/YSZ/Au and Pt/YSZ/Au.

According to the results in Fig. 3, the application of a positive potential on Rh/YSZ/Au led to an electrophobic-type behavior below 360 °C and an inverted volcano-type behavior above 360 °C for both reaction of C_3H_6 oxidation and NO reduction. The electrophobic-type behavior below 360 °C complies with the above explanation and with the conclusions of the previous study [27]. A similar result of the inverted volcano-type behavior at a temperature above 360 °C has been reported where Rh electrode displayed the inverted volcano-type behavior at 430 °C under a gas mixture containing 850 ppm C_3H_6 + 700 ppm NO + 0.3% O_2 [16]. Presumably, a negative potential above 360 °C reduced the Rh electrode by NO electric decomposition [4,5]; however, the negative potential strengthened the chemical bonds with oxygen below 360 °C.

The catalytic activity for both C_3H_6 and NO for Rh/10YSZ/Au was greater than that for Rh/YSZ/Au irrespective of the applied potential (Fig. 5). SEM analysis of the surface morphology of Rh/10YSZ/Au indicates that compared with Rh/YSZ/Au, there is a greater sintering of the Rh electrode and a lower conductivity for Rh electrode with the YSZ substrate (Fig. 9(b)). It is presumed to be the cause for the looseness of the NO electric decomposition reaction for of Rh/10YSZ/Au (Fig. 5(b)), the lower current (Fig. 6(a)), and the lower electric promotion below 300 °C. Due to the low conductivity for Rh electrode for Rh/10YSZ/Au, it was difficult to reduce the Rh electrode to metal state by applying a negative potential. It is unusual that the catalytic activity for Rh/10YSZ/Au is higher than that for Rh/YSZ/Au, because higher sintering of Rh electrode normally induces lower catalytic activity. We suspect that the enough area of bare YSZ without Rh electrode may cause the effective back spillover of oxygen, which weakens the bonds between oxygen and the Rh electrode and reduces the Rh oxide to Rh metal, as determined by XPS (Fig. 10).

First, we expected that the synergistic effect of the PtRh electrode would improve the catalytic activity and the electrochemical behavior. However, the catalytic activity of RhPt/YSZ/Au was lower than that of Rh/YSZ/Au (Fig. 7) and appeared to be caused by the low catalytic activity of Pt/YSZ/Au, as displayed in Fig. 8. When a negative potential was applied to the working electrode, the current of RhPt/YSZ/Au was larger than that of Rh/YSZ/Pt. Based on this fact, it appears that RhPt electrode can be reduced very easily compared with Rh electrode. The easily reduced RhPt electrode resulted in a higher ρ value for C_3H_6 and NO.

We assumed the product of NO reduction was only N_2 as shown in chemical reaction (6). However N_2, N_2O, and NO_2 were expected to be the main products when NO is reduced under oxidizing conditions. We can measure NO_2 but not N_2 and N_2O using the employed setup. N_2 and CO have the same mass number 28; similarly, N_2O and CO_2 have the same mass number 44. Because CO is a product of C_3H_6 oxidation, it interferes with the detection of N_2, while CO_2 interferes with the detection of N_2O. Therefore, we only investigated the NO_2 yield by measuring the peak corresponding to the mass number 46; this is shown in Fig. 13. It was concluded that the maximum rate of NO_2 production was less than a few percent of NO, based on the rough estimation using the mass sensitivity of NO and NO_2 [28], while the production of NO reduction was attributed to N_2 and N_2O. The production of NO_2 increased with an increasing temperature under all the potentials studied. It appears that N_2O increased in case of Rh electrode when applying −2 V, and this increase is presumed to be caused by Faradaic NO oxidation at the Rh electrode.

5. Conclusions

The catalytic activity of Rh/10YSZ/Au was higher than that of Rh/YSZ/Au irrespective of the applied potential. Based on the results obtained using SEM and XPS analysis, we conclude that longer sintering leads to a higher catalyst activity and that opposite effects are true for a given catalytic system. In other words, longer sintering enhances non-Faradaic electrochemical promotion of C_3H_6 oxidation by favoring oxygen spillover, but is disadvantageous to Faradaic electro-reduction of NO due to decrease in electrical conductivity.

The RhPt electrode, which was expected to show catalytic activity by the synergistic effect of Pt and Rh, did not show higher activity than pure Rh electrode, but was reduced more easily and had a higher rate enhancement factor value for C_3H_6 and NO in comparison to pure Rh electrode.

Acknowledgment

The authors thank Professor C.G. Vayenas for helpful discussions and cooperation.

References

[1] K. Kammer, Appl. Catal. B 58 (2005) 33–39.
[2] P. Vernoux, F. Gaillard, C. Lopez, E. Siebert, J. Catal. 217 (2003) 203–208.
[3] X. Li, P. Vernoux, Appl. Catal. B 61 (2005) 267–273.
[4] M. Awano, S. Bredikhin, A. Aronin, G. Abrosimova, S. Katayama, T. Hiramatsu, Solid State Ionics 175 (2004) 605–608.
[5] H. Songa, J. Moona, H. Jin Hwang, J. Eur. Ceram. Soc. 26 (2006) 981–986.
[6] C.G. Vayenas, S. Bebelis, S. Ladas, Nature 343 (1990) 625.

[7] C.G. Vayenas, S. Bebelis, C. Pliangos, S. Brosda, D. Tsiplakides, Electrochemical Activation of Catalysis, Kluwer Academic Publishers/Plenum Press, New York, 2001.
[8] C. Kokkofitis, G. Karagiannakis, S. Zisekas, M. Stoukides, J. Catal. 234 (2005) 476–487.
[9] I. Constantinou, D. Archonta, S. Brosda, M. Lepage, Y. Sakamoto, C.G. Vayenas, J. Catal. 251 (2007) 400–409.
[10] F. Dorado, A.L. Consuegra, C. Jiménez, J.L. Valverde, Appl. Catal. A 321 (2007) 86–92.
[11] S. Matsumoto, H. Shinjoh, Adv. Chem. Eng. 279 (33) (2007) 1–46.
[12] S. Matsumoto, Catal. Today 90 (3–4) (2004) 183–190.
[13] Y. Nagai, T. Hirabayashi, K. Dohmae, N. Takagi, T. Minami, H. Shinjoh, S. Matsumoto, J. Catal. 242 (1) (2006) 103–109.
[14] S. Bebelis, N. Kotsionopoulos, Solid State Ionics 177 (2006) 2205–2209.
[15] C.G. Vayenas, S. Brosda, C. Pliangos, J. Catal. 216 (2003) 487–504.
[16] C. Pliangos, C. Raptis, Th. Badas, C.G. Vayenas, Solid State Ionics 136–137 (2000) 767–773.
[17] A. Gayen, T. Baidya, K. Biswas, S. Roy, M.S. Hegde, Appl. Catal. A 315 (2006) 135–146.
[18] Y. Cai, H.G. Stenger Jr., C.E. Lyman, J. Catal. 161 (1996) 123–131.
[19] R.E. Lakis, Y.P. Cai, H.G. Stenger, C.E. Lyman, J. Catal. 154 (1995) 276–287.
[20] D. Dong, M. Liu, Y. Dong, B. Lin, J. Yang, G. Meng, J. Power Sources 171 (2007) 495–498.
[21] A. Lintanf, E. Djurado, P. Vernoux, Solid State Ionics 178 (2008) 1998–2008.
[22] C.G. Vayenas, S. Brosada, C. Pliangos, J. Catal. 203 (2001) 329.
[23] Z. Hlavathy, P. Tétényi, Surf. Sci. 410 (1998) 39.
[24] S. Bebelis, C.G. Vayenas, J. Catal. 118 (1989) 125.
[25] B. Béguin, F. Gaillard, M. Primet, P. Vernoux, L. Bultel, M. Hénault, C. Roux, E. Siebert, Ionics 2 (2002) 128.
[26] F. Dorado, A. de Lucas-Consuegra, P. Vernoux, J.L. Valverde, Appl. Catal. B 73 (2007) 42.
[27] O. Foti, O. Lavanchy, C. Comminellis, J. Appl. Electrochem. 30 (2000) 1223.
[28] A. Cornu, R. Massot, Comparison of Mass Spectral Data, second ed., Heyden & Son Ltd., London, 1975.